Size-resolved cloud condensation nuclei (CCN) activity and closure analysis at the HKUST Supersite in Hong Kong

J.W. Meng[1], M.C. Yeung[2], Y.J. Li[1,3], B.Y.L. Lee[1], C.K. Chan[1,2,*]

[1]Division of Environment, Hong Kong University of Science and Technology, Clear Water Bay, Hong Kong SAR, China

[2]Department of Chemical and Biomolecular Engineering, The Hong Kong University of Science and Technology Clear Water Bay, Hong Kong SAR, China

[3]Current Address: School of Engineering and Applied Sciences, Harvard University, USA

*Correspondence to: C.K. Chan (keckchan@ust.hk)

Abstract

The cloud condensation nuclei (CCN) properties of atmospheric aerosols were measured on May 1-30, 2011 at a coastal site in Hong Kong. Size-resolved CCN activation curves, the ratio of number concentration of CCN (N_{CCN}) to aerosol concentration (N_{CN}) as a function of particle size, were obtained at supersaturation (SS) = 0.15%, 0.35%, 0.50%, and 0.70% using a DMT CCN counter (CCNc) and a TSI scanning mobility particle sizer (SMPS). The mean bulk size-integrated N_{CCN} ranged from ~500 cm^{-3} at SS = 0.15% to ~2100 cm^{-3} at SS = 0.70%, and the mean bulk N_{CCN}/N_{CN} ratio ranged from 0.16 at SS = 0.15% to 0.65 at SS = 0.70%. The average critical mobility diameters (D_{50}) at SS = 0.15%, 0.35%, 0.50%, and 0.70% were 116 nm, 67 nm, 56 nm, and 46 nm, respectively. The corresponding average hygroscopic parameters (κ_{CCN}) were 0.39, 0.36, 0.31, and 0.28. The decrease in κ_{CCN} can be attributed to the increase in organic to inorganic volume ratio as particle size decreases, as measured by an Aerodyne high resolution time-of-flight aerosol mass spectrometer (HR-ToF-AMS). The κ_{CCN} correlates reasonably well with κ_{AMS_SR} based on size-resolved AMS measurements: $\kappa_{AMS\_SR} = \kappa_{org} \times f_{org} + \kappa_{inorg} \times f_{inorg}$, where f_{org} and f_{inorg} are the organic and inorganic volume fractions, respectively, κ_{org} = 0.1 and κ_{inorg} = 0.6, with a R^2 of 0.51.

In closure analysis, N_{CCN} was estimated by integrating the measured size-resolved N_{CN} for particles larger than D_{50} derived from κ assuming internal mixing state. Estimates using κ_{AMS_SR} show that the measured and predicted N_{CCN} were generally within 10% of each other at all four SS. The deviation increased to 26% when κ_{AMS} was calculated from bulk PM1 AMS measurements of particles because PM1 was dominated by particles of 200 nm to 500 nm in diameter, which had a larger inorganic fraction than those of D_{50} (particle diameter < 200 nm). A constant κ = 0.33 (the average value of κ_{AMS_SR} over the course of campaign) was found to give an N_{CCN} prediction within 12% of the actual measured values. We also compared N_{CCN} estimates based on the measured average D_{50} and the average size-resolved CCN activation ratio to examine the relative importance of hygroscopicity and mixing state. N_{CCN} was found to be relatively more sensitive to the mixing state and hygroscopicity at a high SS = 0.70% and a low SS = 0.15%, respectively.

1 Introduction

Atmospheric aerosols can act as cloud condensation nuclei (CCN) and affect cloud formation by influencing the CCN number concentration (N_{CCN}) and the size of cloud droplets. Whether aerosol particles will eventually form cloud droplets under a set atmospheric condition mainly depends on their size, chemical composition, and mixing states. Predicting N_{CCN} usually involves measuring the aerosol size distribution and making assumptions about the chemical composition associated to mixing state. Bulk chemical compositions and an assumption of internal mixing state (i.e., particles are identical mixtures of all participating species) are often used in predicting N_{CCN} (Moore et al., 2012a; Wang et al., 2010). Ambient aerosols are complex mixtures and the aerosol compositions vary substantially with particle size. The hygroscopicity parameter (κ) is used to represent the effect of chemical composition on CCN activity (Petters and Kreidenweis, 2007, 2013). Size-resolved chemical compositions give a size-dependent κ which leads to better N_{CCN} predictions than those based on bulk compositions (Medina et al., 2007; Stroud et al., 2007; Wang et al., 2010).

While the real-time aerosol size-resolved chemical compositions such as non-refractory (NR)-species and black carbon (BC) can be obtained with an aerosol mass spectrometer and a single particle soot photometer, respectively, information on the mixing state is usually not available or incomplete. Various assumptions have been applied to describe the aerosol mixing state (Asa-Awuku et al., 2011; Bougiatioti et al., 2009; Cubison et al., 2008; Ervens et al., 2010; Lance et al., 2009; Lathem et al., 2013; Moore et al., 2012a; Rose et al., 2011; Wang et al., 2010). N_{CCN} predictions assuming internal mixing are usually larger than measured values by 20% or even more, since this assumption overestimates the contribution of organics to N_{CCN} (Rose et al., 2011; Wang et al., 2010; Wex et al., 2010). Another extreme assumption is external mixing, which is when the aerosol contains different types of particles but each particle consists of a single species (Textor et al., 2006; Zhang et al., 2010). Under this assumption, the number concentration (N_{CN}) of each type of particles is determined as the product of the total N_{CN} and the volume fraction of the species. The D_{50} of a species is calculated based on its κ (Moore et al., 2012a; Wang et al., 2010) and N_{CCN} is obtained by integrating N_{CN} above D_{50}. Finally, the total N_{CCN} is calculated by adding up all the predicted N_{CCN} of the species. This simplified external

84 mixing state assumption could underestimate $N_{CCN.}$ For example, Wang et al. (2010) reported
85 an underestimation of ~20% in N_{CCN} at supersaturation (*SS*) from 0.11% to 0.35%. Aerosol
86 mixing state and chemical composition are thus important factors that need to be considered in
87 the CCN prediction, especially in places where anthropogenic aerosol emission is strong and
88 pollution is heavy (Ervens et al., 2010; Kammermann et al., 2010; Kerminen et al., 2012; Rose
89 et al., 2010; Wang et al., 2010).

90 Recently, measurements of the condensation nuclei (CN) and CCN spectra simultaneously
91 by combining a scanning mobility particle sizer (SMPS) and a CCN counter (CCNc) have been
92 made (Asa-Awuku et al., 2010; Lance et al., 2009; Moore et al., 2012a; Moore et al., 2010;
93 Padró et al., 2010; Rose et al., 2010). The size-resolved CCN activation ratios, i.e., the fraction
94 of the measured N_{CCN}/N_{CN} as a function of particle size, are the combined results of the size
95 distribution, size resolved chemical composition, and the mixing state of the aerosols. Deng et
96 al. (2013) estimated N_{CCN} by integrating the product of the measured size-distributed N_{CN} and
97 the averaged size-resolved CCN activation ratio at each particle size bin measured at Wuqing in
98 the North China Plain. The estimated and measured values differed by less than 6% at *SS* = 0.06%
99 to 0.81%.

100 In recent years, the rapid urbanization and industrial development in the Pearl River Delta
101 (PRD) have resulted in heavy air pollution, especially particulate matter (PM) pollution (Chan
102 and Yao, 2008). Hong Kong, a typical coastal city south-east of the PRD, is affected by PM due
103 to both local anthropogenic emissions and transportation of pollutants from the PRD (Lee et al.,
104 2013).

105 In this study, we report for the first time size-resolved measurements of CCN activity in
106 Hong Kong. We correlated the CCN-derived hygroscopicity (κ_{CCN}) with those estimated from
107 the size-dependent aerosol chemical compositions determined by an Aerodyne high-resolution
108 Time-of-Flight Aerosol Mass Spectrometer (HR-ToF-AMS, hereafter as AMS). Assuming
109 internal mixtures, we carried out closure studies on N_{CCN} prediction based on the size-
110 distributions of N_{CN} measured by a TSI SMPS and on the hygroscopicity values derived from
111 size resolved and size integrated chemical compositions measured by AMS using Köhler theory,

$\kappa_{AMS,}$ and some assumed constants. Finally, using the average D_{50} and the size-resolved CCN activation ratios from the CCN measurements, we examined the relative importance of hygroscopicity and mixing state in N_{CCN} predictions at different *SS*.

2 Experimental methods

2.1 Sampling site and meteorological conditions

Measurements of aerosol chemical properties and CCN activity were carried out throughout the entire month of May 2011 at the Air Quality Research Supersite situated on the campus of the Hong Kong University of Science and Technology (HKUST) on the east coast of Hong Kong (see http://www.envr.ust.hk/research/research-facility/background-materials.html). High relative humidity (*RH*) with a mean of 81% and an average temperature of 26.0 ℃ prevailed in this study. More information on the sampling location and meteorological conditions is available from Lee et al. (2013) and Li et al. (2013).

2.2 Instrument setup

2.2.1 Sample Inlet System

Ambient air was sampled at a flow rate of 16.67 L/min after passing through a PM2.5 cyclone on the roof of the Supersite (appropriately 20 m above sea level) and into a stainless steel sampling port supplying the on-line instruments of the TSI SMPS, the Droplet Measurement Technologies (DMT) dual column continuous-flow CCN counter (CCNc-200) and the Aerodyne AMS. The sampled air passed through a 1-m long diffusion drier (BMI, San Francisco, CA) filled with silica gel, thus its *RH* was below 30% before it went into the above instruments for measurements.

2.2.2 CCN measurements

Size-resolved CCN spectra and activation ratios were measured with the CCNc-200 (Lance et al., 2006; Roberts and Nenes, 2005) coupled with a TSI SMPS, consisting of a differential mobility analyzer (DMA, TSI 3081L) and a water-based condensation particle counter (WCPC, TSI 3785).

As shown in Fig.1, charge-neutralized aerosols passed through the DMA for classification. The classified aerosols were then split into two streams: with one going into the WCPC for N_{CN} measurements and the other into the CCNc-200 for N_{CCN} measurements. The particle size distribution was measured every 6 min, with an up-scan time of 300 s. The sample flow rate was 1 L/min for the DMA, 0.5 L/min for the WCPC and the CCNc-200 each, and the closed-loop sheath air flow rate was 10 L/min. These flow rate settings allow SMPS (DMA+WCPC) measurements for particles ranging from 7 nm to 300 nm in mobility diameter (D_m), which as we will show later, cover the D_{50} (D_m) range of the particles studied. The sheath flow rate was continuously corrected using a mass flow controller. All flow rates were regularly checked and sizing accuracy for the SMPS and the CCNc-200 was verified with Polystyrene latex (PSL) spheres.

The CCNc-200 was operated at a total flow rate of 1 L/min, of which 0.5 L/min was for column A connected to the DMA to measure the size-resolved CCN spectrum and another 0.5 L/min was for column B connected to the sample inlet system to measure the total N_{CCN}. A sheath-to-aerosol flow ratio of 10 was used. Lathem and Nenes (2011) pointed out that the direct measurements could lead to underestimations of bulk N_{CCN} due to the depletion of water inside the column by a large amount of aerosols and recommended the use of size-resolved CCN measurement. In our measurements, the bulk N_{CCN} integrated from size-resolved CCN measurement using column A are usually fewer than 5000 cm^{-3} and they correlate well with that from the direct measurement using column B with a slope of 0.97 and correlation coefficient (R^2) of 0.53 as shown in Fig.S1. We use bulk N_{CCN} calculated from column A for the comparison with N_{CN} from SMPS and for the closure study below. For every measurement cycle, four *SS* (0.15%, 0.35%, 0.50%, and 0.70%) were selected. Measurements at *SS* = 0.15% lasted 22 min whereas those at other *SS* lasted 12 min each for repeatability. CCNc temperature

transients during *SS* changes are known to produce unreliable spectra if they occur during a voltage up-scan (Moore et al., 2010). In our measurements, the instrument profiles were allowed up to ~2 min to stabilize whenever the temperature gradient was changed. At *SS* = 0.15%, a longer time (~4 min) was required for the stabilization of temperatures. Only data collected under stabilized temperatures were used for analysis.

The CCNc-200 was calibrated with size selected DMA ammonium sulfate particles at the four *SS* (Deng et al., 2011; Rose et al., 2008) regularly during the campaign. The instrument *SS* was derived from Köhler theory using a constant van't Hoff factor of 2.5 for ammonium sulfate (Low, 1969; Tang and Munkelwitz, 1994; Young and Warren, 1992).

2.2.3 Aerosol chemical compositions

Non-refractory PM_1 (NR-PM_1) constituents of sulfate, nitrate, ammonium, chloride, and organics were measured with the AMS operated under V, pToF, and W modes. The principle behind the instrument has been described in detail elsewhere (DeCarlo et al., 2006) and will only be briefly described here. In pToF mode, the instrument performs particle sizing based on particle time-of-flight with the aid of a chopper and gives size-resolved chemical composition data in vacuum aerodynamic diameter (D_{va}) (DeCarlo et al., 2004). In V mode, the shorter traveling path for ions in the ion time-of-flight (ToF) chamber gives a mass spectral resolving power of approximately 2000 (DeCarlo et al., 2006) and better sensitivity. In W mode, the mass spectral resolving power is approximately 4000 (DeCarlo et al., 2006) but the signal-to-noise ratio is lower. The instrument was operated alternately between the V+pToF combined mode and the W mode for 5 min each. Evaluation of the ionization efficiency (*IE*) was carried out with ammonium nitrate particles weekly and both the flow rate and particle sizing were calibrated before and after the campaign. A more detailed description of the performance of the AMS during the campaign is presented by Li et al. (2013) and Lee et al. (2013). The AMS only measures NR-species but not elemental carbon (EC), sea salt, or crustal species. However, EC only accounts for less than 5% of the PM1 mass and hence can be neglected (Huang et al., 2014;

Lee et al., 2013). Sea salt and crustal species typically exist in the coarse mode and make negligible contributions to PM1.

2.3 Data analysis

2.3.1 CN and CCN data

The time series of N_{CN} and N_{CCN} distributions were obtained using the TSI Aerosol Instrument Manager (AIM) software (Wang and Flagan, 1989) and CCN acquisition software, respectively. The data collected during the voltage up-scan were employed for the inversion. The Scanning Mobility CCN Analysis (SMCA) was employed for calculating the size-resolved CCN activation fractions (Moore et al., 2010). The ratio of N_{CCN} to N_{CN} gives the size-resolved CCN activation fraction at each size. Then, the size-resolved CCN activation ratio was obtained by fitting the activation fraction with the sigmoidal function described by Equation 1 (see section 2.3.3) (Moore et al., 2010; Padró et al., 2010).

2.3.2 HR-ToF-AMS data

The standard toolkit of SQUIRREL (Sueper, 2011) was used for AMS data analysis. The collection efficiency (*CE*) used for this work was 0.5 and the relative ionization efficiency (*RIE*) of 1.2 for sulfate, 1.1 for nitrate, 1.3 for chloride, 1.4 for organics and 4.0 for ammonium were used as described by Li et al. (2013) and Lee et al. (2013). The size-resolved mass spectra for vacuum aerodynamic diameter (D_{va}) ranging from 50 nm to 2000 nm (DeCarlo et al., 2004) were obtained every 5 min on average. The mass concentration of each size bin was obtained by averaging with the two adjacent size bins to reduce the influence of noise (Rose et al., 2011). In order to relate the size-resolved AMS data with those of SMPS and CCNc measurements directly, the AMS D_{va} size was divided by a factor of 1.7 to obtain the corresponding mobility equivalent diameter (D_m) (Cheng et al., 2006; DeCarlo et al., 2004; Lee et al., 2013). The volume fractions of size-resolved and bulk chemical compositions were calculated from the mass concentrations

using densities of organics and inorganics of 1.3 g cm^{-3} and 1.75 g cm^{-3}, respectively (Alfarra et al., 2006; Cross et al., 2007; Gunthe et al., 2009; King et al., 2007; Lee et al., 2013).

2.3.3 D_{50}, κ_{CCN} and κ_{AMS}

The critical diameter D_{50}, also known as the activation diameter, is the diameter at which 50% of the particles are activated at a specific *SS*. The D_{50} of a simple sigmoidal shaped activation ratio curve is determined by fitting the size-resolved activation fractions with the equation below:

$$\frac{N_{CCN}}{N_{CN}} = \frac{B}{1+\left(\frac{D_p}{D_{50}}\right)^c} \quad (1)$$

where D_p is the dry mobility diameter, *B*, *c*, and D_{50} are fitting coefficients that describe the asymptote/plateau, the slope, and the inflection point of the sigmoid, respectively (Moore et al., 2010; Padró et al., 2012). The values of B were more than 90% during the whole campaign, indicating most of the particles were in the internal mixing state (Mei et al., 2013).

The measured hygroscopic parameter (κ_{CCN}) is determined from D_{50} by:

$$\kappa_{CCN} = \frac{4A^3\sigma_{s/a}^3(T)}{27T^3D_{50}^3\ln^2 S_c} \quad (2)$$

where A = 8.69251×10^{-6} Km^3J^{-1}, $\sigma_{s/a}(T)$ is the temperature-dependent surface tension of the solution/air interface, T is temperature and S_c is the critical saturation ratio. Pure water surface tension is assumed in the calculations of κ_{CCN} in this paper (Petters and Kreidenweis, 2013; Sullivan et al., 2009).

The hygroscopic parameter κ_{AMS} can be obtained from AMS measurements using

$$\kappa_{AMS} = \kappa_{org} \times f_{org} + \kappa_{inorg} \times f_{inorg} \quad (3)$$

where f_{org} and f_{inorg} are the organics and inorganics volume fraction derived from AMS measurements (Petters and Kreidenweis, 2007). Bulk κ_{AMS} (hereafter κ_{AMS_B}) and size-resolved κ_{AMS} (hereafter κ_{AMS_SR}) are obtained from the corresponding bulk and size-resolved volume

fractions of organics and inorganics, respectively. Also, it was assumed that κ_{inorg} = 0.6 for the whole campaign, κ_{org} = 0.2 for the hazy period and κ_{org} = 0.1 for the foggy and non-episode periods.

The time-series hygroscopicities derived from bulk and size-resolved AMS measurements are shown in Fig.S2. κ_{AMS_B} were larger than κ_{AMS_SR} in all four *SS* because bulk AMS compositions biased towards the inorganics as discussed below. Their difference increases as *SS* increases because the corresponding D_{50} decreases and these smaller particles have a larger difference in organic fraction than the bulk has.

3 Results and discussion

3.1 Overview

Fig.2 shows an overview of the bulk N_{CCN} concentrations and N_{CCN}/N_{CN} activation ratio at *SS* of (a) 0.15%, (b) 0.35%, (c) 0.50%, and (d) 0.70%, as well as (e) the bulk N_{CN} and the NR-PM1 total and component mass concentration and (f) the volume fractions of the AMS chemical components over the entire month of May 2011. Statistics of the measurements are given in Table I. The gaps in the data in Fig.2 are due to instrument downtime. For most of the time, the total N_{CCN} at *SS* of 0.15%, 0.35%, 0.50% and 0.70% were below 800 cm^{-3}, 3000 cm^{-3}, 5000 cm^{-3} and 5600 cm^{-3} respectively, and N_{CN} was below 10000 cm^{-3}. Both N_{CCN} and N_{CN} in this study are lower than those observed in July 2006 in Guangzhou (Rose et al., 2010). Large fluctuations in the bulk N_{CCN}/N_{CN} ratios were also observed. The bulk N_{CCN}/N_{CN} ratio was as low as 0.03 at *SS* = 0.15%, but it was as high as 0.92 at *SS* = 0.70%. Even at the same *SS*, the bulk N_{CCN}, N_{CN} and N_{CCN}/N_{CN} ratio varied greatly during the campaign.

The bulk mass concentrations of NR-PM1 ranged from 0.8 μg m^{-3} to 72.4 μg m^{-3} with a mean value of 14.5 ± 9.7 μg m^{-3} as shown in Fig.2e. The average bulk volume fractions of NR-species were 53 ± 10%, 25 ± 13% , 18 ± 4%, 4 ± 3% for sulfate, organics, ammonia, and nitrate, respectively (Lee et al., 2013). The bulk mass concentrations for all NR-species were in general

low during the campaign compared with those reported for the PRD region (Gong et al., 2012; Rose et al., 2011; Takegawa et al., 2009; Xiao et al., 2011).

There were two periods of particular interest during this campaign: one was a foggy period (May 15) and the other was a hazy period (May 28-30). The division of the month of May in 2011 into foggy, hazy and non-episode periods was based on differences in meteorology, such as RH, temperature and cloud cover, and mass concentration and the O:C ratio. On average, the foggy period had a high RH (91.1%), a low temperature (23.3 ^{o}C) and a high percentage cloud coverage (89.7%) and a high liquid water content (LWC) in fine particles (47.5 μg m^{-3}) as shown in Li et al. (2013). The hazy period had a much lower RH (66.6%), a higher temperature (26.2 ^{o}C) and a much lower percentage cloud coverage (43.3%) and LWC (17.5 μg m^{-3}). The slowing surface winds and the establishment of a well-defined land-sea breeze with a gradual daily reversal of wind direction contributed to the accumulation of local and regional pollutants coming from the PRD due to the persistent northerly and northwesterly air masses (Lee et al., 2013).

During the foggy period, the bulk NR-PM1 was as high as 30 μg m^{-3} (Fig. 2e; Li et al., 2013). The hazy period was much less humid and it saw the highest mass concentration of NR-PM1 species recorded during the whole campaign. The highest degree of oxygenation with average O:C ratio of 0.51 was also obtained (Li et al., 2013). During the hazy period, the mean bulk N_{CCN} ranged from 1100 cm^{-3} with bulk N_{CCN}/N_{CN} of 0.22 at SS = 0.15% to 5300 cm^{-3} with bulk N_{CCN}/N_{CN} of 0.72 at SS = 0.70%. During non-episode periods, the mean bulk N_{CCN} ranged from 300 cm^{-3} with bulk N_{CCN}/N_{CN} of 0.14 at SS = 0.15% to 2700 cm^{-3} with bulk N_{CCN}/N_{CN} of 0.61 at SS = 0.70%.

3.2 f, κ_{CCN} and κ_{AMS}

The average size-resolved mass distributions and volume fractions (f) of NR-PM1 calculated from AMS measurements are shown in Fig.3a-c and Fig.3d-f, respectively, for the foggy period, the hazy period, and the non-episode periods. The NR-PM1 showed a major mode at the dry

particle size (D_m, hereafter, diameters shown are D_m) of ~285 nm in the foggy period, at ~355 nm in the hazy period and at ~325 nm in the non-episode periods. Sulfate and organics accounted for large mass fractions (78% in total) during the whole campaign as shown in Table II. Sulfate dominated in the foggy period, contributing to a volume fraction of 0.45 for 42-200 nm particles. Organics and nitrate often had a shoulder at a small size mode at 100 nm to 130 nm. This shoulder was obvious in the hazy period and non-episode periods but not so in the foggy period. On average, this smaller mode accounted for 11% and 12% of organics and nitrate, respectively. On the other hand, only 2% of sulfate was found in this mode (Lee et al., 2013).

Fig.3d-f show the average size-resolved volume fraction distributions of the AMS aerosol compositions from 42 nm to 200 nm in the foggy period, the hazy period and the non-episode periods. The volume fraction of organics decreased while the inorganics increased with particle size. Overall, the size-resolved volume fractions of organics ranged from 0.73 at 42 nm to 0.25 at 200 nm. Additionally, the bulk volume ratio of organics to inorganics between 42 nm and 200 nm was 0.65 in the foggy period, 1.33 in the hazy period, and 0.87 in the non-episode periods.

The measured κ_{CCN} (yellow symbols) and the calculated κ_{AMS_SR} (blue symbols), in the form of median values and interquartile ranges, are plotted against their corresponding D_{50} in Fig.3d-f. The median and mean values of κ_{CCN} and κ_{AMS_SR} were essentially the same. Overall, the median D_{50} were 116 nm, 68 nm, 55 nm, and 47 nm, with an interquartile range of less than 16%, at *SS* of 0.15%, 0.35%, 0.50%, and 0.70%, respectively. During the foggy period, which featured high inorganics volume fractions, the median κ_{CCN} were 0.44, 0.37, 0.36 and 0.29 at *SS* from 0.15% to 0.70%. They are higher than the corresponding values in the hazy period (0.38, 0.36, 0.32 and 0.28) and the non-episode periods (0.39, 0.37, 0.33 and 0.27). The difference in κ_{CCN} was most obvious at *SS* = 0.15%, at which D_{50} was around 110 nm, and the corresponding inorganic volume fraction was 0.6 in foggy period, 0.4 in the hazy period and 0.5 in the non-episode period. The high inorganic volume fraction results in high aerosol hygroscopicity.

The κ_{AMS_SR} calculated from Equation 3 assuming κ_{org} = 0.1 and κ_{inorg} = 0.6 agreed well with the measured κ_{CCN} in the foggy period and the non-episode periods as shown in Fig. 3d and f. In the hazy period (Fig.3e), assuming κ_{org} =0.2 and κ_{inorg} = 0.6 gave better agreement between

κ_{AMS_SR} and κ_{CCN}. The hazy period had a higher O:C ratio of 0.51, compared to 0.43 and 0.39 in foggy and the non-episode periods respectively (Li et al., 2013), leading to a higher hygroscopicity of the organic aerosols (Chang et al., 2010; Lambe et al., 2011; Massoli et al., 2010; Mei et al., 2013; Moore et al., 2012b).

We further examine the correlations between the observed κ_{CCN} and the size-resolved organic volume fraction (f_{org}) in Fig.4a for the hazy period and Fig.4b for the rest of the campaign. In order to avoid the negatively impact of low signal-to-noise ratios of AMS measurements on the correlation study, only data points with mass concentrations in a size bin of larger than 0.6 μg m^{-3} were used. Extrapolation of the least square fit line in Fig.4a and Fig.4b to f_{org} =1 yields κ_{org} = 0.21 ± 0.02 and 0.09 ± 0.01 for the organic fraction and extrapolation to f_{org} = 0 yields κ_{inorg} = 0.59 ± 0.03 and 0.59 ± 0.01 for the inorganic fraction, respectively. These values are close to the characteristic values of organic (0.1) and inorganic hygroscopicity (0.6) in the PRD region (Rose et al., 2011), and to the averaged values of κ_{org} = 0.1 and κ_{inorg} = 0.6 - 0.7 in earlier studies in Beijing and the Gulf of Mexico (Gunthe et al., 2011; Moore et al., 2012b). The average organic hygroscopicity is within the typical range for individual organic species from zero for insoluble organics to 0.3 for soluble organics (Hersey et al., 2011; Lambe et al., 2011; Petters and Kreidenweis, 2007). κ_{AMS_SR} correlates reasonably well with κ_{CCN}, with R^2 of 0.51, as shown in Fig.S3.

On the other hand, the mean value of κ_{AMS_B} derived from bulk AMS compositions was 0.45 at *SS* = 0.15% and 0.46 for the other *SS*, which are significantly larger than the measured κ_{CCN} ranging from 0.39 to 0.28 for *SS* of 0.15% to 0.7% as shown in Table IV. Size-resolved AMS measurements are needed to accurately determine the hygroscopicity parameter and predict N_{CCN} (Cubison et al., 2008; Moore et al., 2012a). For closure analysis shown below, we use κ_{org} = 0.1 and κ_{inorg} = 0.6.

3.3 CCN closure study

The closure studies on N_{CCN} prediction were carried out based on the measured size-resolved N_{CN} distributions and the AMS measurements. In the first approach, we assumed internal mixing and used κ_{AMS} from (i) bulk and (ii) the size-resolved AMS measurements for each dataset in Equation 3, and (iii) assumed constant κ values. The corresponding individual D_{50} was then calculated from these κ estimates using Equation 2, based on which N_{CCN} was predicted. Furthermore, we also used the average D_{50} over the whole campaign in N_{CCN} prediction. Table III summarizes the assumptions and parameters used in these methods. In these cases N_{CCN} was calculated by integrating the measured size-resolved N_{CN} distributions for particles larger than D_{50}. The aim of using the average D_{50} was to test how well it represented the activation properties of aerosol during the campaign. Finally, we examined the relative importance of hygroscopicity and mixing state in N_{CCN} predictions at different *SS* by comparing the N_{CCN} using the average D_{50} with an internal mixing assumption and the size-resolved CCN activation ratios from CCN measurements which reflect the actual mixing state of the aerosols. The last approach involved integrating the product of the measured size-distribution of N_{CN} and the size-resolved CCN activation ratio in each particle size bin.

3.3.1 Prediction of N_{CCN} based on κ_{AMS}

3.3.1.1 κ_{AMS} from bulk AMS measurements

The hygroscopicity κ_{AMS_B} was estimated by assuming that all particles have the same chemical composition as determined by bulk AMS measurements and $\kappa_{org} = 0.1$ and $\kappa_{inorg} = 0.6$. The closure results are shown in Fig.5i a-h and Table IV. Overall, the approaches of using individual D_{50} and the average D_{50} grossly over-predicted N_{CCN} by up to 21% and 26%, respectively. As shown in Fig.3a-c, PM1 was dominated by inorganic species with the bulk volume fraction as high as 69% during the whole period. The bulk volume ratio mainly reflects the composition of particles from 200 to 500 nm where inorganic species dominated. On the other hand, D_{50} at the four *SS* were all less than 200 nm where organic species accounted for more than 39% of bulk volume fraction as shown in Table II and Fig.3. Therefore, deriving κ_{AMS} from bulk AMS measurements leads to a positive bias toward inorganic species, and hence an

overestimation of κ_{AMS_B} and N_{CCN}. Wang et al. (2010) found that the overestimation arising from the use of the bulk mass concentrations decreased from 80% to 39% when *SS* decreased from 0.35% to 0.11%. Our data also shows decreasing overestimation as *SS* decreases, except for data at *SS* = 0.15%, where the N_{CCN} was smaller than 1000 cm^{-3} most of the time. The low counts may have introduced larger uncertainty in the measurements as shown in SI.

3.3.1.2 κ_{AMS} from size-resolved AMS measurements

Fig.5ii a-d and e-h show the correlations between the measured N_{CCN} and the N_{CCN} predicted from the individual D_{50} of each data set and the averaged D_{50} derived from κ_{AMS_SR}, respectively. The slope and R^2 are given in Table IV. In general, the N_{CCN} prediction deviated by 10% or less for both approaches and the average D_{50} adequately reflects the aerosol activation properties. At *SS* = 0.70%, individual D_{50} and the average D_{50} gave the close deviations of 10% and 9% respectively between the measured and predicted N_{CCN}. At high *SS*, where even particles of moderate hygroscopicity are activated (Kim et al., 2011), the N_{CCN} prediction is less sensitive to hygroscopicity than at low *SS*. The difference of the deviations increased as *SS* decreased from 0.70% to 0.35%. At lower *SS*, differences in hygroscopicity as reflected from the different D_{50} used in the calculations gave larger differences in N_{CCN} predictions.

The overestimation from using the average D_{50} decreased from 9% at SS of 0.70% (D_{50} = 46 nm) to 5% and 1% at *SS* of 0.50% (D_{50} = 56 nm) and 0.35% (D_{50} = 67 nm), respectively. The fraction of non/less-hygroscopic hydrocarbon-like organic aerosols (HOA) decreased with increasing particle size (Lee et al., 2013). They contribute little to N_{CCN} by themselves but the assumption of internal mixing allows them to contribute to CCN due to their mixing with more hygroscopic species and leads to an overestimated N_{CCN} (Rose et al., 2011; Wang et al., 2010). Size-resolved EC was not available and EC might also have caused the overestimation in N_{CCN} prediction. When *SS* decreased, D_{50} increased and the impact of HOA on the N_{CCN} predictions decreased because of their smaller abundance relative to the hygroscopic inorganics. The large deviation in N_{CCN} prediction at *SS* = 0.15% may be due to the uncertainty in the low number

counts of CCN measurements or the high sensitivity of N_{CCN} to hygroscopicity at low *SS* as discussed later.

3.3.2 Prediction of N_{CCN} from the constant κ

A constant κ = 0.30 has been proposed for predicting N_{CCN} and understanding the indirect effects of continental aerosols on climate on a global modeling scale (Andreae and Rosenfeld, 2008; Pringle et al., 2010). Rose et al. (2011) showed that the deviations between the measured and predicted N_{CCN} were less than 20% when they used an averaged κ = 0.30 over the course of their campaign in PRD in 2006. We evaluated the use of constant κ = 0.30, 0.33 (the average κ_{AMS_SR} over the campaign at the four *SS*), and 0.35 to estimate N_{CCN}. Overall, using κ = 0.35 overestimated N_{CCN} at all four *SS* while using 0.33 and 0.30 underestimated it at low *SS* ≤ 0.35% and overestimated it at high *SS* ≥ 0.50%, respectively, as shown in Fig.S4 and Table IV. The slopes for κ = 0.30, 0.33 and 0.35 are quite different (0.91, 0.98 and 1.05) at *SS* = 0.15%, while they are much closer (1.11, 1.12 and 1.13) at *SS* = 0.70%. The difference in N_{CCN} prediction for the three κ decreased gradually from 14% at *SS* = 0.15% to 2% at *SS* = 0.70%. These results further confirm that the prediction of N_{CCN} is less sensitive to κ at high *SS* than at low one, and that the impact of hygroscopicity on the N_{CCN} prediction decreases with increasing *SS*.

The difference in the sensitivity of predicted N_{CCN} to hygroscopicity at different *SS* can also be attributed to the aerosol size distributions (Dusek et al., 2006; Ervens et al., 2007). The average aerosol size distribution over the whole period had a main mode at ~70 nm and a shoulder at ~30 nm (Fig.6a) in this campaign. At *SS* = 0.15%, D_{50} is approximately 116 nm and on the right of the main mode (Fig.6b), a slight variation of κ and D_{50} will cause a large change in N_{CCN} prediction. On the contrary, at *SS* = 0.70%, the corresponding D_{50} = 46 nm is on the left of the main mode (Fig.6c), a variation of κ and D_{50} will have less impact on N_{CCN} prediction as the N_{CCN} is dominated by the mode at 70 nm.

In addition, we carried out the N_{CCN} prediction during the hazy period, when HOA contributes to ~25% of OA (Li et al, 2013), based on the average size-resolved (1) κ_{AMS} = 0.33

over the whole campaign period and (2) κ_{AMS} = 0.35 over the hazy period only. As shown in Fig. S5, using κ_{AMS} = 0.33 and 0.35 gave similar results with overestimations of 14% and 13% at *SS* = 0.70% respectively. In the hazy period, the assumption of internal mixing state allowed HOA containing particles to act as CCN, thereby resulting in an overestimation of N_{CCN} by up to 14%. At *SS* = 0.15%, using κ = 0.33 led to an overestimation of just 2%, while an overestimation of 9% was found when using κ = 0.35. Overall, using κ = 0.33 gave predictions of N_{CCN} (Table IV) comparable to those using the κ_{AMS_SR} and better than those using κ_{AMS_B} at all four *SS*.

3.3.3 Mixing state and hygroscopicity

As discussed earlier, closure analysis based on hygroscopicity or D_{50} derived from chemical compositions alone cannot account for variability in the mixing state of aerosols, which could cause significant differences between predicted and measured N_{CCN}. In this section, we first calculate N_{CCN} by integrating the measured size-resolved N_{CN} distributions above the average D_{50}, obtained from the average CCN size-resolved activation ratio over the whole campaign. The second method involves integrating the product of the measured size-distribution of N_{CN} and the average size-resolved N_{CCN}/N_{CN} activation ratio in each particle size bin. The size-resolved N_{CCN}/N_{CN} activation ratios reflect the influences of both the size-resolved chemical compositions and mixing state on CCN activity, and thus can potentially exclude the impact of non/less hygroscopicity species on N_{CCN} prediction and be used to examine the relative importance of mixing state and hygroscopicity in closure analysis compared to predictions assuming internal mixing state (Deng et al., 2013). The first method involves the hygroscopicity of aerosols as reflected by the value of D_{50} and the assumption of internal mixing while the second method involves hygroscopicity with actual mixing state information imbedded in the measured activation ratio curves. A comparison of the predictions of these two methods would give hints to the role of assumption of mixing states. The average size-resolved CCN activation ratios at the four *SS* over the whole campaign are shown in Fig.S6. Data points are shown as means ± standard deviations.

458 The correlations of measured and predicted N_{CCN} based on the average D_{50} (a-d) and the
459 average size-resolved activation ratio (e-h) are shown in Fig.5 iii a-d and e-h. The slopes of the
460 fitted lines and R^2 at different *SS* are given in Table IV. The predicted and the measured N_{CCN}
461 differed by less than 10% using the average D_{50}. The difference is comparable to those using the
462 average D_{50} from κ_{AMS_SR} (Fig.5ii e-h). At *SS* = 0.70%, using the average size-resolved CCN
463 activation ratios reduced the overestimation from 8% when using the average D_{50} to 4%. As
464 discussed above, the sensitivity of the N_{CCN} prediction to hygroscopicity is low at *SS* = 0.70%,
465 where a large change of 25% in hygroscopicity from 0.28 to 0.35 result in only a variation within
466 5% in N_{CCN} (Table IV). From the AMS measurements, the portion of non/less-hygroscopic
467 species inferred by the fractions of f_{43} and f_{57} increased as the particle size decreased (Lee et al.,
468 2013). Because of their higher abundance, their mixing with the hygroscopic components has a
469 higher impact at *SS* = 0.70% (D_{50} = 46 nm) than that at low *SS* = 0.15% (D_{50} = 116 nm), where
470 the reduction in the overestimation is minimal, from 10% when using the average D_{50} to 9%
471 when using the average activation ratios approach. On the contrary, a difference of 19% was
472 found when hygroscopicity increased from 0.30 to 0.39 at this low *SS*.

473 The average size-resolved activation ratios during the hazy, foggy and non-episode periods
474 at *SS*=0.15% and 0.7% are shown in Fig. 7. At *SS*=0.15%, the activation ratios during the hazy
475 and non-episode periods are similar but it is higher during the foggy period due possibly to the
476 higher volume fraction of inorganics (Fig. 3d-f) and the smaller amount of non/less hygroscopic
477 organics (Li et al., 2013). At *SS*=0.70%, the CCN activation ratios of particles ranging from 50
478 nm to 100 nm in size are lower in the hazy period than in the non-episode period. The difference
479 in the trends at *SS*=0.15% and 0.70% may be due to the larger fractions of non/less hygroscopic
480 species in smaller particles in the hazy period. These particles, which constitute a larger fraction
481 of OA in the hazy period than in the other periods, likely formed external mixtures containing
482 the aged particles of sulfate and the more oxidized (and hygroscopic) organics. Hence, a larger
483 difference in the activation ratios between the hazy and the other periods could be observed at
484 *SS*=0.70% than at *SS*=0.15%.

Fig. 8 shows the N_{CCN} predicted based on the average D_{50} and the average size-resolved CCN activation ratio over the hazy period. At *SS* = 0.15%, using the average CCN activation ratio reduces overestimation from 12% when using average D_{50} to 10%. However, a much larger reduction from 8% to 1% was found at *SS* = 0.70%. This comparison further suggests that a change in mixing state affects N_{CCN} prediction more at high *SS* than at the low *SS* and that N_{CCN} prediction is more sensitive to mixing state at high *SS* than hygrocopicity.

4 Conclusion

In this study, a DMT CCNc-200 for N_{CCN} measurement, a TSI SMPS for N_{CN} measurement, and an Aerodyne HR-ToF-AMS for size-resolved and bulk PM1 chemical composition measurement were used to investigate the size-resolved CCN activity at a coastal site in Hong Kong in May 2011. Closure studies were carried out based on the κ_{AMS} estimated from bulk and size-resolved AMS measurement assuming internal mixing state. The deviation of N_{CCN} predicted from the individual D_{50} obtained from κ_{AMS} was similar to that predicted from the average D_{50} over the whole period at the four *SS*, which indicates that the average D_{50} well represented the aerosol CCN activation properties in this study. using κ_{AMS_B} grossly over-predicted N_{CCN} by up to 26% because of the positive bias toward the inorganic fraction. On the contrary, the N_{CCN} prediction based on κ_{AMS_SR} was within 10% of the measurements. An accurate description of κ incorporating size-dependent compositions is necessary for good N_{CCN} predictions.

We compared the sensitivity of the N_{CCN} prediction to hygroscopicity (based on assumed internal mixing and κ estimates) and mixing state at different *SS*. N_{CCN} was found to be more sensitive to hygroscopicity than to mixing state at *SS* = 0.15% but the reverse is true at *SS* = 0.70%. At *SS* = 0.15%, D_{50} (116nm) is larger than the mode diameter of the typical aerosol distributions we observed. A slight variation in κ (and D_{50}) would have a larger effect on N_{CCN} prediction than would at high *SS* = 0.70%, where D_{50} (46 nm) is smaller than the mode diameter. The effect of mixing state is larger at *SS* = 0.70%, which is associated with smaller particles

having a higher percentage of non/less-hygroscopic components, than at *SS* = 0.15%. Hygroscopicity is relatively less important to N_{CCN} prediction at this high *SS*.

5 Acknowledgments

This work was supported by the University Grants Committee (Special Equipment Grant, SEG-HKUST07), Research Grants Council (GRF 600413) and the Environmental Conservation Funds (ECF) of Hong Kong (project number: ECWW09EG04).

References

Alfarra, M. R., Paulsen, D., Gysel, M., Garforth, A. A., Dommen, J., Prévôt, A. S., Worsnop, D. R., Baltensperger, U., and Coe, H.: A mass spectrometric study of secondary organic aerosols formed from the photooxidation of anthropogenic and biogenic precursors in a reaction chamber, Atmos. Chem. Phys., 6, 5279-5293, doi:10.5194/acp-6-5279-2006, 2006.

Andreae, M.,O and Rosenfeld, D.: Aerosol–cloud–precipitation interactions. Part 1. The nature and sources of cloud-active aerosols, Earth-Sci. Rev., 89, 13-41, 2008.

Asa-Awuku, A., Nenes, A., Gao, S., Flagan, R. C., and Seinfeld, J. H.: Water-soluble SOA from Alkene ozonolysis: composition and droplet activation kinetics inferences from analysis of CCN activity, Atmos. Chem. Phys., 10, 1585-1597, doi:10.5194/acp-10-1585-2010, 2010.

Asa-Awuku, A., Moore, R. H., Nenes, A., Bahreini, R., Holloway, J. S., Brock, C. A., Middlebrook, A. M., Ryerson, T. B., Jimenez, J. L., and DeCarlo, P. F.: Airborne cloud condensation nuclei measurements during the 2006 Texas Air Quality Study, J. Geophys. Res-Atmos., 116, D11201, doi:10.1029/2010jd014874, 2011.

Bougiatioti, A., Fountoukis, C., Kalivitis, N., Pandis, S., Nenes, A., and Mihalopoulos, N.: Cloud condensation nuclei measurements in the marine boundary layer of the Eastern Mediterranean: CCN closure and droplet growth kinetics, Atmos. Chem. Phys., 9, 7053-7066, doi:10.5194/acp-9-7053-2009, 2009.

Chan, C. K. and Yao, X.: Air pollution in mega cities in China, Atmos. Environ., 42, 1-42, 2008.

Chang, R. Y-W., Slowik, J. G, Shantz, N. C., Vlasenko, A., Liggio, J., Sjostedt, S. J., Leaitch, W. R., and Abbatt, J. P. D.: The hygroscopicity parameter (κ) of ambient organic aerosol at a field site subject to biogenic and anthropogenic influences: relationship to degree of aerosol oxidation, Atmos. Chem. Phys., 10, 5047-5064, doi:10.5194/acp-10-5047-2010, 2010.

Cheng, Y. F., Eichler, H., Wiedensohler, A., Heintzenberg, J., Zhang, Y. H., Hu, M., Herrmann, H., Zeng, L. M., Liu, S., and Gnauk, T.: Mixing state of elemental carbon and non-light-absorbing aerosol components derived from in situ particle optical properties at Xinken in Pearl River Delta of China, J. Geophys. Res-Atmos., 111, D20204, doi: 10.1029/2005jd006929, 2006.

Cross, E. S., Slowik, J. G., Davidovits, P., Allan, J. D., Worsnop, D. R., Jayne, J. T., Lewis†, D. K., Canagaratna, M., and Onasch, T. B.: Laboratory and ambient particle density determinations using light scattering in conjunction with aerosol mass spectrometry, Aerosol Sci. Technol., 41, 343-359, 2007.

Cubison, M. J., Ervens, B., Feingold, G., Docherty, K. S., Ulbrich, I. M., Shields, L., Prather, K., Hering, S., and Jimenez, J. L.: The influence of chemical composition and mixing state of Los Angeles urban aerosol on CCN number and cloud properties, Atmos. Chem. Phys., 8, 5649-5667, doi:10.5194/acp-8-5649-2008, 2008.

DeCarlo, P. F., Kimmel, J. R., Trimborn, A., Northway, M. J., Jayne, J. T., Aiken, A. C., Gonin, M., Fuhrer, K., Horvath, T., Docherty, K. S., Worsnop, D. R., and Jimenez, J. L.: Field-deployable, high-resolution, time-of-flight aerosol mass spectrometer, Anal. Chem., 78, 8281-8289, 2006.

DeCarlo, P. F., Slowik, J. G., Worsnop, D. R., Davidovits, P., and Jimenez, J. L.: Particle morphology and density characterization by combined mobility and aerodynamic diameter measurements. Part 1: Theory, Aerosol Sci. Technol., 38, 1185-1205, 2004.

Deng, Z. Z., Zhao, C. S., Ma, N., Liu, P. F., Ran, L., Xu, W. Y, Chen, J., Liang, Z., Liang, S., Huang, M. Y., Ma, X. C., Zhang, Q., Quan, J. N., Yan, P., Henning, S., Mildenberger, K., Sommerhage, E., Schäfer, M., Stratmann, F., and Wiedensohler, A.: Size-resolved and bulk

activation properties of aerosols in the North China Plain, Atmos. Chem. Phys., 11, 3835-3846, doi:10.5194/acp-11-3835-2011, 2011.
Deng, Z. Z., Zhao, C. S., Ma, N., Ran, L., Zhou, G. Q., Lu, D. R., and Zhou, X. J.: An examination of parameterizations for the CCN number concentration based on in situ measurements of aerosol activation properties in the North China Plain, Atmos. Chem. Phys., 13, 6227-6237, doi:10.5194/acp-13-6227-2013, 2013.
Dusek, U., Frank, G. P., Hildebrandt, L., Curtius, J., Schneider, J., Walter, S., Chand, D., Drewnick, F., Hings, S., Jung, D., Borrmann. S., and Andreae, M. O.: Size matters more than chemistry for cloud-nucleating ability of aerosol particles, Science, 312, 1375-1378, 2006.
Ervens, B., Cubison, M., Andrews, E., Feingold, G., Ogren, J., Jimenez, J., Quinn, P., Bates, T., Wang, J., and Zhang, Q.: CCN predictions using simplified assumptions of organic aerosol composition and mixing state: a synthesis from six different locations, Atmos. Chem. Phys., 10, 4795-4807, doi:10.5194/acp-10-4795-2010, 2010.
Ervens, B., Cubison, M. J., Andrews, E., Feingold, G., Ogren, J. A., Jimenez, J. L., Quinn, P. K., Bates, T. S., Wang, J., Zhang, Q., Coe, H., Flynn, M., and Allan, J. D.: Prediction of cloud condensation nucleus number concentration using measurements of aerosol size distributions and composition and light scattering enhancement due to humidity, J. Geophys. Res., 112, D10S32, doi:10.1029/2006JD007426, 2007.
Gong, Z., Lan, Z., Xue, L., Zeng, L., He, L., and Huang, X.: Characterization of submicron aerosols in the urban outflow of the central Pearl River Delta region of China, Front. Environ. Sci. Eng., 6, 725-733, 2012.
Gunthe, S. S., King, S. M., Rose, D., Chen, Q., Roldin, P., Farmer, D. K., Jimenez, J. L.,Artaxo, P., Andreae, M. O., Martin, S. T., and Pöschl, U.: Cloud condensation nuclei in pristine tropical rainforest air of Amazonia: size-resolved measurements and modeling of atmospheric aerosol composition and CCN activity, Atmos. Chem. Phys., 9, 7551-7575, 2009.
Gunthe, S. S., Rose, D., Su, H., Garland, R. M., Achtert, P., Nowak, A., Wiedensohler, A., Kuwata, M., Takegawa, N., Kondo, Y., Hu, M., Shao, M., Zhu, T., Andreae, M. O., and Pöschl, U.: Cloud condensation nuclei (CCN) from fresh and aged air pollution in the megacity region of Beijing, Atmos. Chem. Phys., 11, 11023-11039, doi:10.5194/acp-11-11023-2011, 2011.
Hersey, S. P., Craven, J. S., Schilling, K. A., Metcalf, A. R., Sorooshian, A., Chan, M. N., Flagan, R. C., and Seinfeld, J. H.: The Pasadena Aerosol Characterization Observatory (PACO): chemical and physical analysis of the Western Los Angeles basin aerosol, Atmos. Chem. Phys., 11, 7417–7443, doi:10.5194/acp-11-7417-2011, 2011.
Huang, X. H., Bian, Q., Ng, W. M., Louie, P. K., and Yu, J. Z.: Characterization of PM 2.5 Major Components and Source Investigation in Suburban Hong Kong: A One Year Monitoring Study, Aerosol Air Qual. Res., 14, 237-250, 2014.
Kammermann, L., Gysel, M., Weingartner, E., Herich, H., Cziczo, D. J., Holst, T., Svenningsson, B., Arneth, A., and Baltensperger, U.: Subarctic atmospheric aerosol composition: 3. Measured and modeled properties of cloud condensation nuclei, J. Geophys. Res., 115, D04202, doi:10.1029/2009JD012447, 2010.
Kerminen, V.-M., Paramonov, M., Anttila, T., Riipinen, I., Fountoukis, C., Korhonen, H., Asmi, E., Laakso, L., Lihavainen, H., and Swietlicki, E.: Cloud condensation nuclei production associated with atmospheric nucleation: a synthesis based on existing literature and new results, Atmos. Chem. Phys., 12, 12037-12059, doi:10.5194/acp-12-12037-2012, 2012.
Kim, J. H., Yum, S. S., Shim, S., Yoon, S.-C., Hudson, J. G., Park, J., and Lee, S.-J.: On aerosol hygroscopicity, cloud condensation nuclei (CCN) spectra and critical supersaturation measured

623 at two remote islands of Korea between 2006 and 2009, Atmos. Chem. Phys., 11, 12627-12645,
624 doi:10.5194/acp-11-12627-2011, 2011.
625 King, S. M., Rosenoern, T., Shilling, J. E., Chen, Q., and Martin, S. T.: Cloud condensation
626 nucleus activity of secondary organic aerosol particles mixed with sulfate, Geophys. Res. Lett.,
627 34, L24806, doi:10.1029/2007GL030390, 2007.
628 Lambe, A. T., Onasch, T. B., Massoli, P., Croasdale, D. R., Wright, J. P., Ahern, A. T., Williams, L.
629 R., Worsnop, D. R., Brune, W. H., and Davidovits, P.: Laboratory studies of the chemical
630 composition and cloud condensation nuclei (CCN) activity of secondary organic aerosol (SOA)
631 and oxidized primary organic aerosol (OPOA), Atmos. Chem. Phys., 11, 8913-8928,
632 doi:10.5194/acp-11-8913-2011, 2011.
633 Lance, S., Nenes, A., Mazzoleni, C., Dubey, M. K., Gates, H., Varutbangkul, V., Rissman, T. A.,
634 Murphy, S. M., Sorooshian, A., and Flagan, R. C.: Cloud condensation nuclei activity, closure,
635 and droplet growth kinetics of Houston aerosol during the Gulf of Mexico Atmospheric
636 Composition and Climate Study (GoMACCS), J. Geophys. Res., 114, D00F15,
637 doi:10.1029/2008JD011699, 2009.
638 Lance, S., Nenes, A., Medina, J., and Smith, J. N.: Mapping the operation of the DMT continuous
639 flow CCN counter, Aerosol Sci. Technol., 40, 242-254, 2006.
640 Lathem, T. L., Beyersdorf, A. J., Thornhill, K. L., Winstead, E. L., Cubison, M. J., Hecobian, A.,
641 Jimenez, J. L., Weber, R. J., Anderson, B. E., and Nenes, A.: Analysis of CCN activity of Arctic
642 aerosol and Canadian biomass burning during summer 2008, Atmos. Chem. Phys., 13, 2735-
643 2756, doi:10.5194/acp-13-2735-2013, 2013.
644 Lathem, T. L. and Nenes, A.: Water vapor depletion in the DMT continuous-flow CCN chamber:
645 Effects on supersaturation and droplet growth, Aerosol Sci. Technol., 45, 604-615, 2011.
646 Lee, B. P., Li, Y. J., Yu, J. Z., Louie, P. K., and Chan, C. K.: Physical and chemical
647 characterization of ambient aerosol by HR-ToF-AMS at a suburban site in Hong Kong during
648 springtime 2011, J. Geophys. Res.-Atmos., 118, 8625-8639, doi:10.1002/jgrd.50658, 2013.
649 Li, Y. J., Lee, B. Y. L., Yu, J. Z., Ng, N. L., and Chan, C. K.: Evaluating the degree of oxygenation
650 of organic aerosol during foggy and hazy days in Hong Kong using high-resolution time-of-
651 flight aerosol mass spectrometry (HR-ToF-AMS), Atmos. Chem. Phys., 13, 8739-8753,
652 doi:10.5194/acp-13-8739-2013, 2013.
653 Low, R. D. H.: A generalized equation for the solution effect in droplet growth, J. Atmos. Sci., 26,
654 608-611, 1969.
655 Massoli, P., Lambe, A. T., Ahern, A. T., Williams, L. R., Ehn, M., Mikkila, J., Canagaratna, M. R.,
656 Brune, W. H., Onasch, T. B., Jayne, J. T., Petaja, T., Kulmala, M., Laaksonen, A., Kolb, C. E.,
657 Davidovits, P., and Worsnop, D. R.: Relationship between aerosol oxidation level and
658 hygroscopic properties of laboratory generated secondary organic aerosol (SOA) particles,
659 Geophys. Res. Lett., 37, L24801, doi:10.1029/2010gl045258, 2010.
660 Medina, J., Nenes, A., Sotiropoulou, R. E. P., Cottrell, L. D., Ziemba, L. D., Beckman, P. J., and
661 Griffin, R. J.: Cloud condensation nuclei closure during the International Consortium for
662 Atmospheric Research on Transport and Transformation 2004 campaign: Effects of size-resolved
663 composition, J. Geophys. Res., 112, D10s31, doi:10.1029/2006jd007588, 2007.
664 Mei, F., Setyan, A., Zhang, Q., and Wang, J.: CCN activity of organic aerosols observed downwind
665 of urban emissions during CARES, Atmos. Chem. Phys., 13, 12155-12169, doi:10.5194/acp-13-
666 12155-2013, 2013.

667 Moore, R. H., Cerully, K., Bahreini, R., Brock, C. A., Middlebrook, A. M., and Nenes, A.:
668 Hygroscopicity and composition of California CCN during summer 2010, J. Geophys. Res.-
669 Atmos., 117, D00v12, doi:10.1029/2011jd017352, 2012a.
670 Moore, R. H., Nenes, A., and Medina, J.: Scanning mobility CCN analysis-A method for fast
671 measurements of size-resolved CCN distributions and activation kinetics, Aerosol Sci. Technol.,
672 44, 861-871, 2010.
673 Moore, R. H., Raatikainen, T., Langridge, J. M., Bahreini, R., Brock, C. A., Holloway, J. S., Lack,
674 D. A., Middlebrook, A. M., Perring, A. E., Schwarz, J. P., Spackman, J. R., and Nenes, A.: CCN
675 spectra, hygroscopicity, and droplet activation kinetics of secondary organic aerosol resulting
676 from the 2010 Deepwater Horizon oil spill, Environ. Sci. Technol., 46, 3093-3100, 2012b.
677 Padró, L. T., Moore, R. H., Zhang, X., Rastogi, N., Weber, R. J., and Nenes, A.: Mixing state and
678 compositional effects on CCN activity and droplet growth kinetics of size-resolved CCN in an
679 urban environment, Atmos. Chem. Phys., 12, 10239-10255, doi:10.5194/acp-12-10239-2012,
680 2012.
681 Padró, L. T., Tkacik, D., Lathem, T., Hennigan, C. J., Sullivan, A. P., Weber, R. J., Huey, L. G.,
682 and Nenes, A.: Investigation of cloud condensation nuclei properties and droplet growth kinetics
683 of the water - soluble aerosol fraction in Mexico City, J. Geophys. Res.-Atmos, 115, D09204,
684 doi:10.1029/2009jd013195, 2010.
685 Petters, M. D. and Kreidenweis, S. M.: A single parameter representation of hygroscopic growth
686 and cloud condensation nucleus activity, Atmos. Chem. Phys., 7, 1961-1971, doi:10.5194/acp-8-
687 6273/2008, 2007.
688 Petters, M. D. and Kreidenweis, S. M.: A single parameter representation of hygroscopic growth
689 and cloud condensation nucleus activity-Part 3: Including surfactant partitioning, Atmos. Chem.
690 Phys., 13, 1081-1091, doi:10.5194/acp-13-1081-2013, 2013.
691 Pringle, K. J., Tost, H., Pozzer, A., Pöschl, U., and Lelieveld, J.: Global distribution of the effective
692 aerosol hygroscopicity parameter for CCN activation, Atmos. Chem. Phys., 10, 5241-5255,
693 doi:10.5194/acp-10-5241-2010, 2010.
694 Roberts, G. C. and Nenes, A.: A continuous-flow streamwise thermal-gradient CCN chamber for
695 atmospheric measurements, Aerosol Sci. Technol., 39, 206-221, 2005.
696 Rose, D., Gunthe, S. S., Mikhailov, E., Frank, G. P., Dusek, U., Andreae, M. O., and Pöschl, U.:
697 Calibration and measurement uncertainties of a continuous-flow cloud condensation nuclei
698 counter (DMT-CCNC): CCN activation of ammonium sulfate and sodium chloride aerosol
699 particles in theory and experiment, Atmos. Chem. Phys., 8, 1153-1179, doi:10.5194/acp-8-1153-
700 2008, 2008.
701 Rose, D., Gunthe, S. S., Su, H., Garland, R. M., Yang, H., Berghof, M., Cheng, Y. F.,Wehner, B.,
702 Achtert, P., Nowak, A., Wiedensohler, A., Takegawa, N., Kondo, Y., Hu, M., Zhang, Y.,
703 Andreae, M. O., and Pöschl, U.: Cloud condensation nuclei in polluted air and biomass burning
704 smoke near the mega-city Guangzhou, China–Part 2: Size-resolved aerosol chemical
705 composition, diurnal cycles, and externally mixed weakly CCN-active soot particles, Atmos.
706 Chem. Phys., 11, 2817-2836, doi:10.5194/acp-11-2817-2011, 2011.
707 Rose, D., Nowak, A., Achtert, P., Wiedensohler, A., Hu, M., Shao, M., Zhang, Y., Andreae, M. O.,
708 and Pöschl, U.: Cloud condensation nuclei in polluted air and biomass burning smoke near the
709 mega-city Guangzhou, China-Part 1: Size-resolved measurements and implications for the
710 modeling of aerosol particle hygroscopicity and CCN activity, Atmos. Chem. Phys., 10, 3365-
711 3383, doi:10.5194/acp-10-3365-2010, 2010.

Stroud, C. A., Nenes, A., Jimenez, J. L., DeCarlo, P. F., Huffman, J. A., Bruintjes, R., Nemitz, E., Delia, A. E., Toohey, D. W., Guenther, A. B., and Nandi, S.: Cloud activating properties of aerosol observed during CELTIC, J. Atmos. Sci., 64, 441-459, 2007.

Sueper, D.: ToF-AMS data analysis software: http://cires.colorado.edu/jimenez-group/ToFAMSResources/ToFSoftware/index.html, (last access: 1 June, 2012), 2011.

Sullivan, R. C., Moore, M. J. K., Petters, M. D., Kreidenweis, S. M., Roberts, G. C., and Prather, K. A.: Effect of chemical mixing state on the hygroscopicity and cloud nucleation properties of calcium mineral dust particles, Atmos. Chem. Phys., 9, 3303-3316, doi:10.5194/acp-9-3303-2009, 2009.

Takegawa, N., Miyakawa, T., Watanabe, M., Kondo, Y., Miyazaki, Y., Han, S., Zhao, Y., Van Pinxteren, D., Bruggemann, E., Gnauk, T., Herrmann, H., Xiao, R., Deng, Z., Hu, M., Zhu, T., and Zhang, Y.: Performance of an Aerodyne aerosol mass spectrometer (AMS) during intensive campaigns in China in the summer of 2006, Aerosol Sci. Technol., 43, 189-204, 2009.

Tang, I. N. and Munkelwitz, H. R.: Water activities, densities, and refractive indices of aqueous sulfates and sodium nitrate droplets of atmospheric importance, J. Geophys. Res.-Atmos, 99, 18801-18818, doi:10.1029/94jd01345, 1994.

Textor, C., Schulz, M., Guibert, S., Kinne, S., Balkanski, Y., Bauer, S., Berntsen, T., Berglen, T., Boucher, O., Chin, M., Dentener, F., Diehl, T., Easter, R., Feichter, H., Fillmore, D., Ghan, S., Ginoux, P., Gong, S., Grini, A., Hendricks, J., Horowitz, L., Huang, P., Isaksen, I., Iversen, I., Kloster, S., Koch, D., Kirkevåg, A., Kristjansson, J. E., Krol, M., Lauer, A., Lamarque, J. F., Liu, X., Montanaro, V., Myhre, G., Penner, J., Pitari, G., Reddy, S., Seland, Ø., Stier, P., Takemura, T., and Tie, X.: Analysis and quantification of the diversities of aerosol life cycles within AeroCom, Atmos. Chem. Phys., 6, 1777-1813, doi:10.5194/acp-6-1777-2006, 2006.

Wang, J., Cubison, M. J., Aiken, A. C., Jimenez, J. L., and Collins, D. R.: The importance of aerosol mixing state and size-resolved composition on CCN concentration and the variation of the importance with atmospheric aging of aerosols, Atmos. Chem. Phys., 10, 7267-7283, doi:10.5194/acp-10-7267-2010, 2010.

Wang, S. C. and Flagan, R. C.: Scanning electrical mobility spectrometer, Aerosol Sci. Technol., 13, 230-240, 1990.

Wex, H., McFiggans, G., Henning, S., and Stratmann, F.: Influence of the external mixing state of atmospheric aerosol on derived CCN number concentrations, Geophys. Res. Lett., 37, L10805, doi:10.1029/2010gl043337, 2010.

Xiao, R., Takegawa, N., Zheng, M., Kondo, Y., Miyazaki, Y., Miyakawa, T., Hu, M., Shao, M., Zeng, L., Gong, Y., Lu, K., Deng, Z., Zhao, Y., and Zhang, Y. H.: Characterization and source apportionment of submicron aerosol with aerosol mass spectrometer during the PRIDE-PRD 2006 campaign, Atmos. Chem. Phys., 11, 6911-6929, doi:10.5194/acp-11-6911-2011, 2011.

Young, K. C. and Warren, A. J.: A reexamination of the derivation of the equilibrium supersaturation curve for soluble particles, J. Atmos. Sci., 49, 1138-1143, 1992.

Zhang, Z., Engling, G., Lin, C.-Y., Chou, C. C.-K., Lung, S.-C. C., Chang, S.-Y., Fan, S., Chan, C.-Y., and Zhang, Y.-H.: Chemical speciation, transport and contribution of biomass burning smoke to ambient aerosol in Guangzhou, a mega city of China, Atmos. Environ., 44, 3187-3195, 2010.

Table I. Statistics of the bulk N_{CCN} (cm^{-3}) at four *SS* (%) showing the minimum, maximum, mean number concentration, the N_{CCN}/N_{CN} ratio, and standard deviation (SD). The last column shows the number of samples (*n*) in this campaign.

SS (%)	Max		Min		Mean ± SD		*n*
	N_{CCN} (cm^{-3})	N_{CCN}/N_{CN}	N_{CCN} (cm^{-3})	N_{CCN}/N_{CN}	N_{CCN} (cm^{-3})	N_{CCN}/N_{CN}	
0.15	2815	0.54	33	0.03	512 ± 452	0.16 ± 0.08	319
0.35	8055	0.78	186	0.08	1546 ± 1137	0.48 ± 0.14	316
0.50	9156	0.82	210	0.12	1815 ± 1285	0.57 ± 0.14	326
0.70	9268	0.92	280	0.16	2082 ± 1484	0.65 ± 0.14	320

Table II. The average size-resolved mass concentrations (μg m^{-3}, Conc.) and volume fractions (*f*) of chemical compositions from size-resolved AMS measurements during the foggy, hazy and the non-episode periods. Conc. and *f* were obtained by integrating over the size range (D_m) from 42 nm to 1200 nm for Fig.3a-c and from 42 nm to 200 nm for Fig.3d-f. Data are shown as mean ± standard deviations.

Period	Organics		Sulfate		Ammonium		Nitrate		Chloride	
	Conc.	*f*	Conc.	*f*	Conc.	*f*	Conc.	*f*	Conc.	*f*
Foggy	1.60 ±1.10	0.39 ±0.12	4.86 ±3.51	0.45 ±0.10	1.33 ±0.98	0.14 ±0.04	0.18 ±0.12	0.03 ±0.00	0.03 ±0.02	0.001 ±0.00
Hazy	4.25 ±2.52	0.57 ±0.08	5.96 ±4.36	0.29 ±0.06	1.71 ±1.22	0.08 ±0.03	0.51 ±0.27	0.06 ±0.01	0.02 ±0.01	0.002 ±0.00
The rest	1.19 ±0.71	0.47 ±0.11	2.65 ±1.86	0.37 ±0.08	0.81 ±0.55	0.12 ±0.03	0.25 ±0.15	0.04 ±0.00	0.02 ±0.01	0.002 ±0.00

Table III. Methods used in N_{CCN} prediction based on the individual and average D_{50} over whole period from AMS measurement.

Methods	Mixing state	Chemical composition	κ_{AMS}	D_{50}
I	Internal	Bulk AMS measurements	$\kappa_{AMS} = 0.1 \times f_{org} + 0.6 \times f_{inorg}$	Individual
II	Internal	Bulk AMS measurements		Average
III	Internal	Size-resolved AMS measurements		Individual
IV	Internal	Size-resolved AMS measurements		Average
V	Internal	N/A	0.35/0.33/0.30	Constants

Table IV. Overview of N_{CCN} predictions, κ from D_{50} based on CCN measurement and derived from equation 3 based on AMS measurement are shown as mean ± standard deviation, slope and R^2 are from the least square fit between the calculated N_{CCN} and measured ones.

Categories	Principles	*SS* (%)	κ	Slope	R^2
CCN_C	The average D_{50} from CCN measurement	0.15	0.39 ± 0.06	1.10	0.94
		0.35	0.36 ± 0.09	1.01	0.95
		0.50	0.31 ± 0.10	1.05	0.97
		0.70	0.28 ± 0.09	1.08	0.98
	The average CCN activation ratio	0.15	-	1.09	0.94
		0.35	-	0.99	0.95
		0.50	-	1.02	0.97
		0.70	-	1.04	0.98
AMS	The D_{50} from κ_{AMS_B}	0.15	-	1.21	0.93
		0.35	-	1.06	0.95
		0.50	-	1.13	0.96
		0.70	-	1.17	0.98
	The average D_{50} from κ_{AMS_B}	0.15	0.45 ± 0.07	1.26	0.93
		0.35	0.46 ± 0.06	1.08	0.96
		0.50	0.46 ± 0.06	1.13	0.96
		0.70	0.46 ± 0.07	1.18	0.98
	The D_{50} from κ_{AMS_SR}	0.15	-	1.06	0.91
		0.35	-	0.94	0.93
		0.50	-	1.03	0.95
		0.70	-	1.10	0.97
	The average D_{50} from κ_{AMS_SR}	0.15	0.37 ± 0.07	1.08	0.94
		0.35	0.35 ± 0.08	1.01	0.95
		0.50	0.31 ± 0.07	1.05	0.97
		0.70	0.29 ± 0.09	1.09	0.98
Others	Constant κ	0.15	0.35/0.33/0.30	1.05/0.98/0.91	0.95/0.95/0.95
		0.35	0.35/0.33/0.30	1.01/0.96/0.91	0.95/0.95/0.95
		0.50	0.35/0.33/0.30	1.08/1.05/1.03	0.97/0.97/0.97
		0.70	0.35/0.33/0.30	1.13/1.12/1.11	0.98/0.98/0.98

Figure Captions

Fig.1. Schematic of the experimental setup for size-resolved CCN activation and chemical composition measurement.

Fig.2. The N_{CCN} and the N_{CCN}/N_{CN} ratio at *SS* of (a) 0.15%, (b) 0.35%, (c) 0.50%, and (d) 0.70%; (e) N_{CN} and NR-species mass concentrations from CCNc, SMPS and AMS; (f) NR-species volume fractions derived from AMS.

Fig.3. Size-resolved mass concentration distributions of aerosol chemical composition derived from AMS averaged over (a) the foggy period, (b) the hazy period, and (c) the non-episode periods; the corresponding size-resolved volume fractions of aerosol chemical compositions (colored areas), the observed κ_{CCN} (yellow) and the calculated κ_{AMS_SR} (blue) during (d) the foggy period, (e) the hazy period and (g) the non-episode period. Data points median values and interquartile ranges. $\kappa_{inorg} = 0.6$ in all cases, $\kappa_{org} = 0.1$ in (d) and (f), $\kappa_{org} = 0.2$ in (e).

Fig.4. Correlations between the observed κ_{CCN} and the organic volume fraction (f_{org}) determined by size-resolved AMS measurements for the (a) hazy period ($n = 72$) and (b) the non-episode period ($n = 516$). The red line is the linear least squares fit (p-value < 0.01) shown in figure.

Fig.5. Calculations of N_{CCN} based on i (a-d) the individual D_{50} and (e-h) the average D_{50} over the whole period from κ_{AMS_B}, ii (a-d) the individual D_{50} and (e-h) the average D_{50} over the whole period from κ_{AMS_SR} and iii (a-d) the average D_{50} and (e-h) the average size-resolved CCN activation ratio from CCN measurement over the whole period.

Fig.6. The average aerosol size distribution over the whole period (a), N_{CCN} prediction based on D_{50} at *SS* of (b) 0.15% and (c) 0.70%. Data points are mean values and standard deviation.

Fig.7. The average size-resolved CCN activation ratio at *SS* of (a) 0.15% and (b) 0.70% during the hazy, foggy and non-episode periods.

Fig.8. N_{CCN} estimation in hazy period based on (a and b) the average D_{50} and (c and d) the average size-resolved CCN activation ratio from CCN measurement over the hazy period.

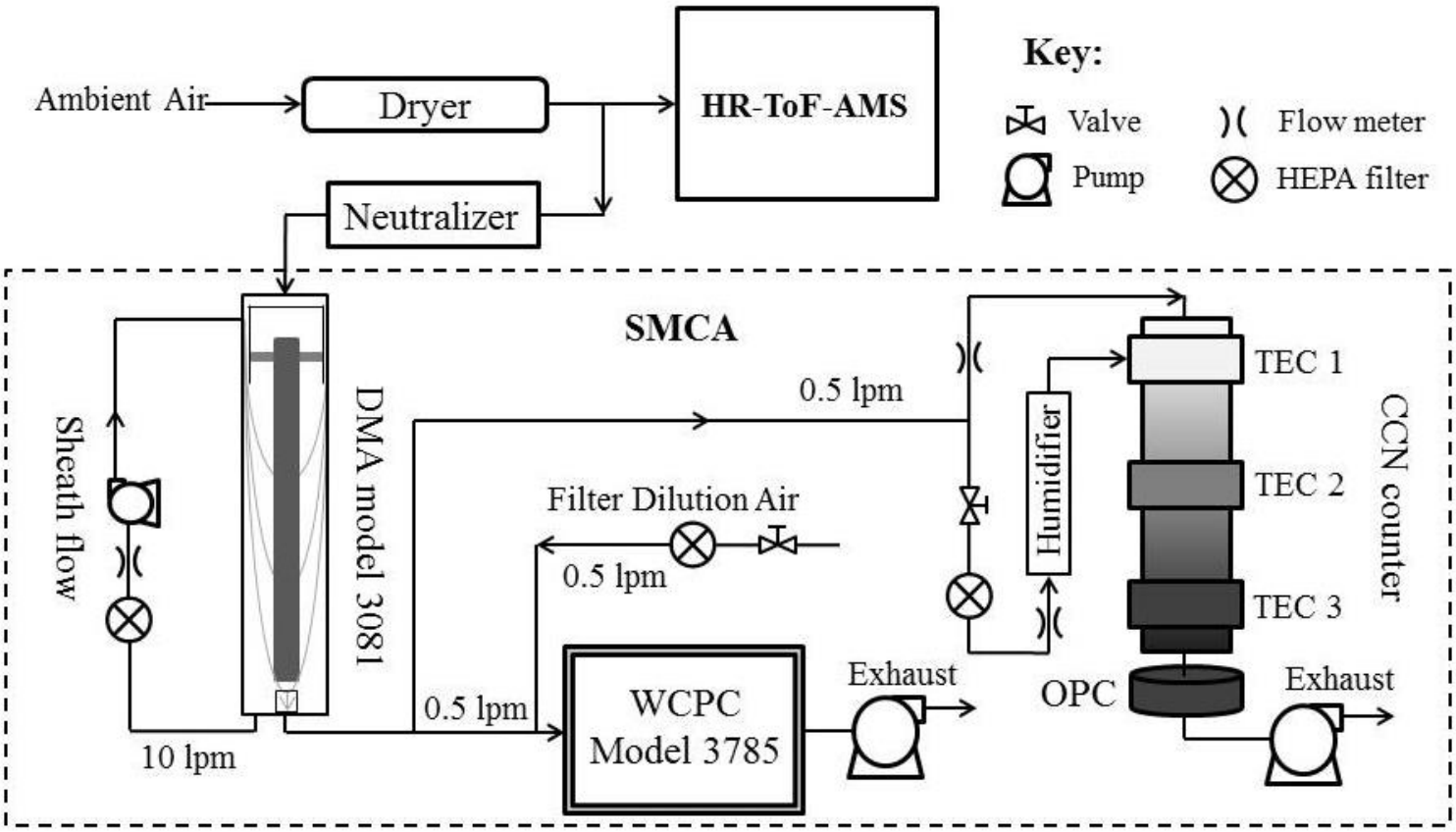

848

849

850

851

852

853

854

855

856 Fig.1. Schematic of the experimental setup for size-resolved CCN activation and chemical
857 composition measurement.

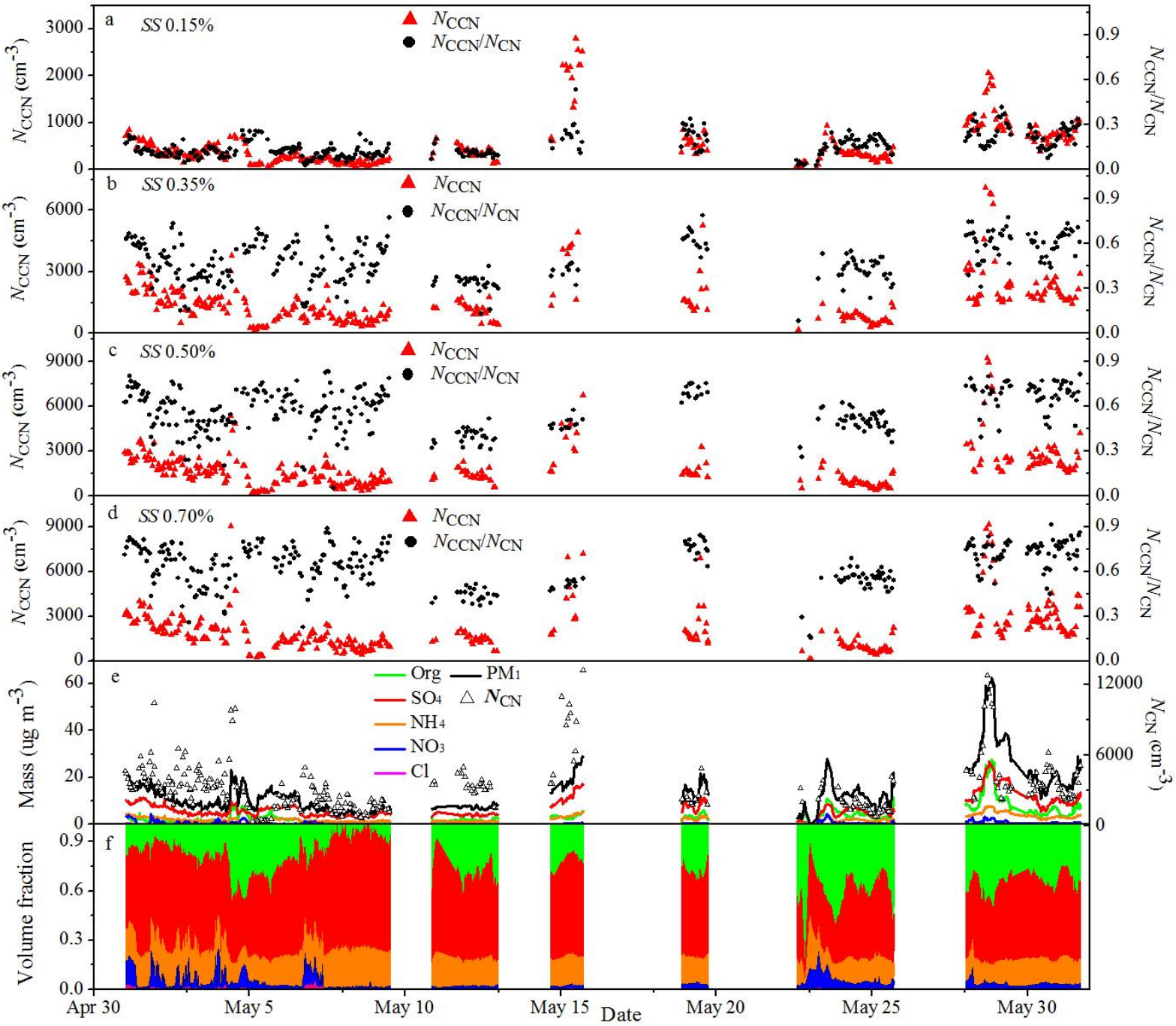

858

859

860 Fig.2. The N_{CCN} and the N_{CCN}/N_{CN} ratio at *SS* of (a) 0.15%, (b) 0.35%, (c) 0.50%, and (d) 0.70%; (e)
861 N_{CN} and NR-species mass concentration derived from CCNc, SMPS and AMS respectively; (f) NR-
862 species volume fraction derived from AMS.

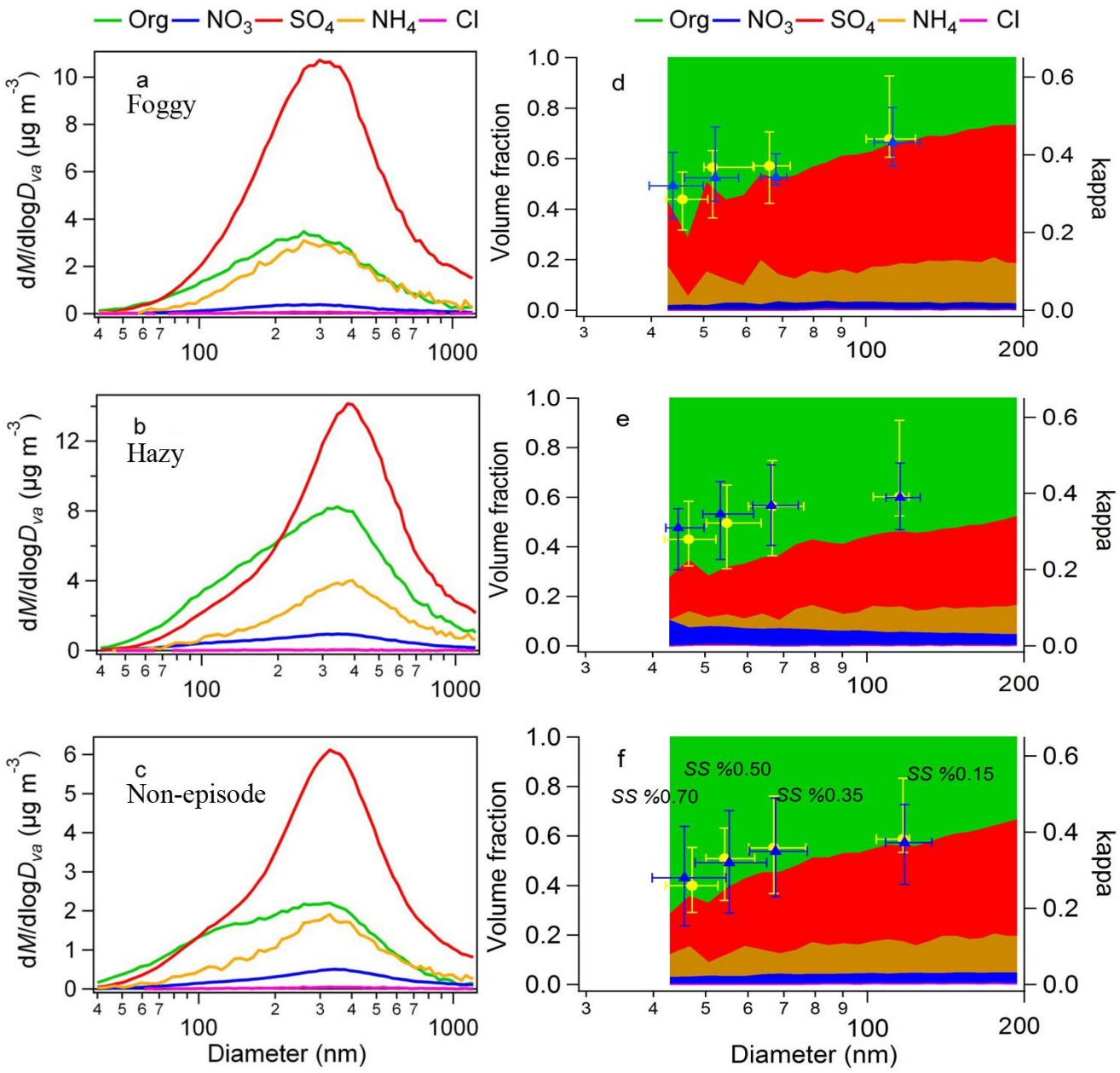

863

864

865 Fig.3. Size-resolved mass concentration distributions of aerosol chemical composition derived
866 from AMS averaged over (a) the foggy period, (b) the hazy period, and (c) the non-episode
867 periods; the corresponding size-resolved volume fractions of aerosol chemical compositions
868 (colored areas) and the observed κ_{CCN} (yellow) and the calculated κ_{AMS_SR} (blue) during (d) the
869 foggy period, (e) the hazy period and (f) the non-episode period. Data points are median values
870 and interquartile ranges. κ_{inorg} = 0.6 in all cases, κ_{org} = 0.1 in (d) and (f), and κ_{org} = 0.2 in (e).

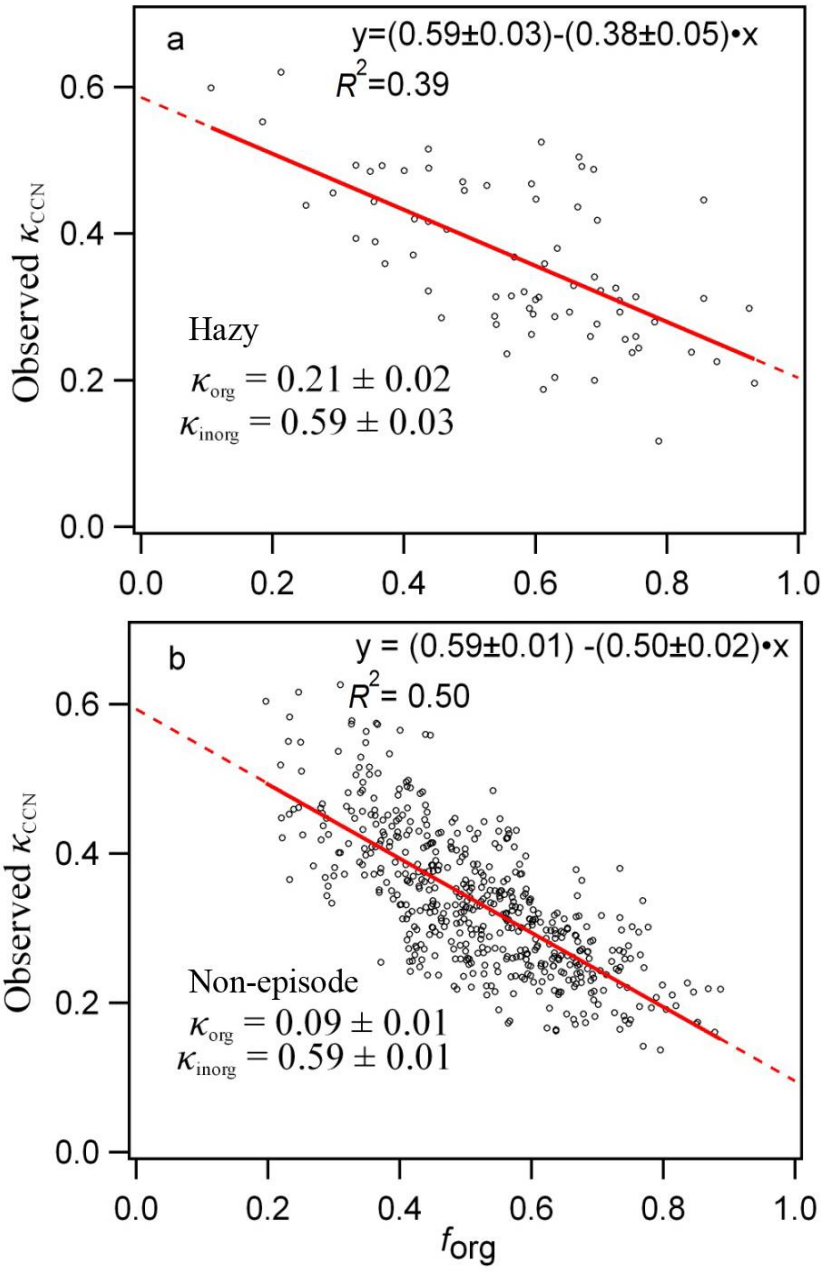

Fig.4. Correlations between the observed κ_{CCN} and the organic volume fraction (f_{org}) determined by size-resolved AMS measurements for the (a) hazy period (n = 72) and (b) the non-episode period (n = 516). The red line is the linear least squares fit (p-value < 0.01) shown in figure.

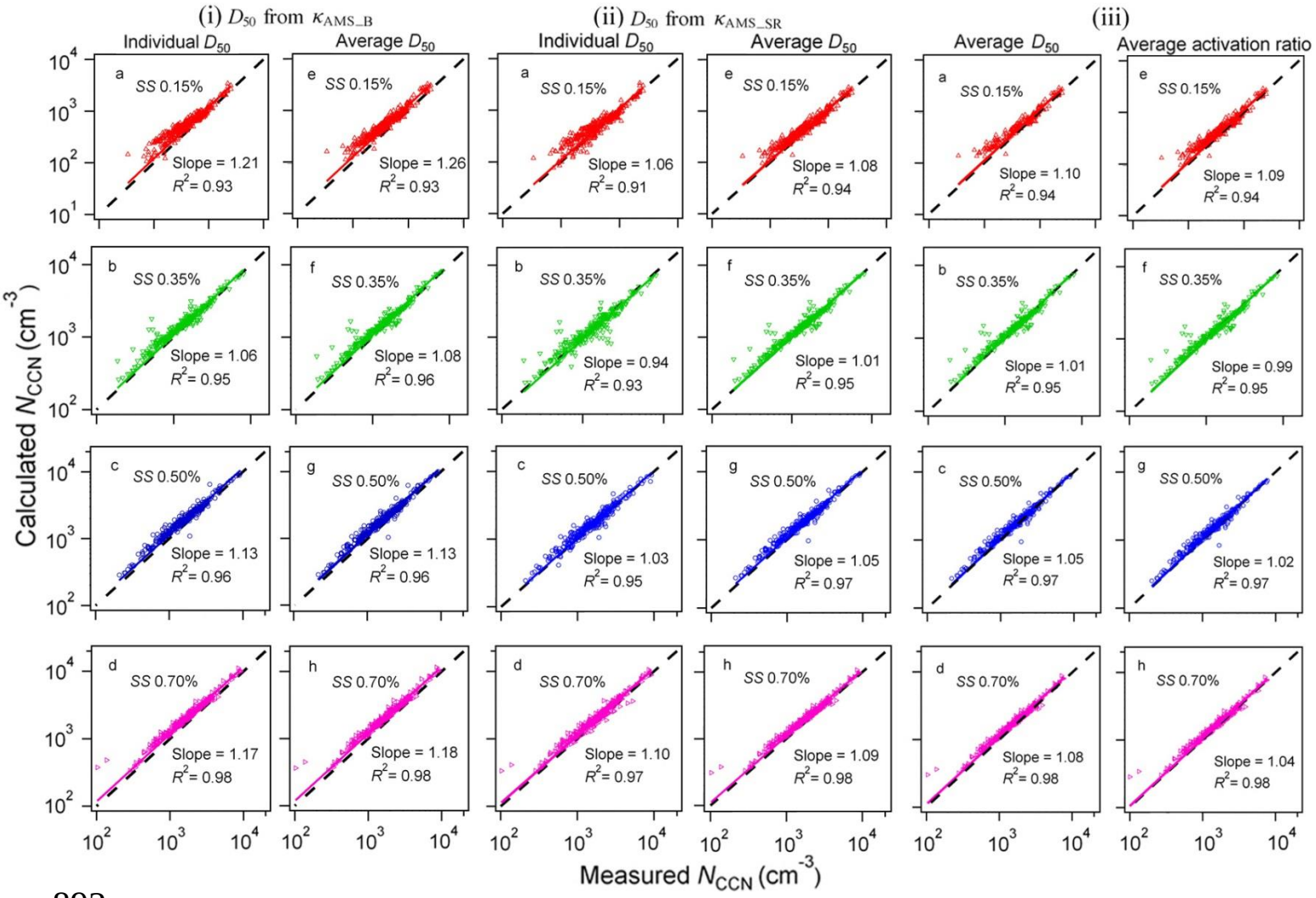

Fig.5. Predictions of N_{CCN} based on i (a-d) the individual D_{50} and (e-h) the average D_{50} over the whole period from κ_{AMS_B}, ii (a-d) the individual D_{50} and (e-h) the average D_{50} over the whole period from κ_{AMS_SR} and iii (a-d) the average D_{50} and (e-h) the average size-resolved CCN activation ratio from CCN measurement over the whole period.

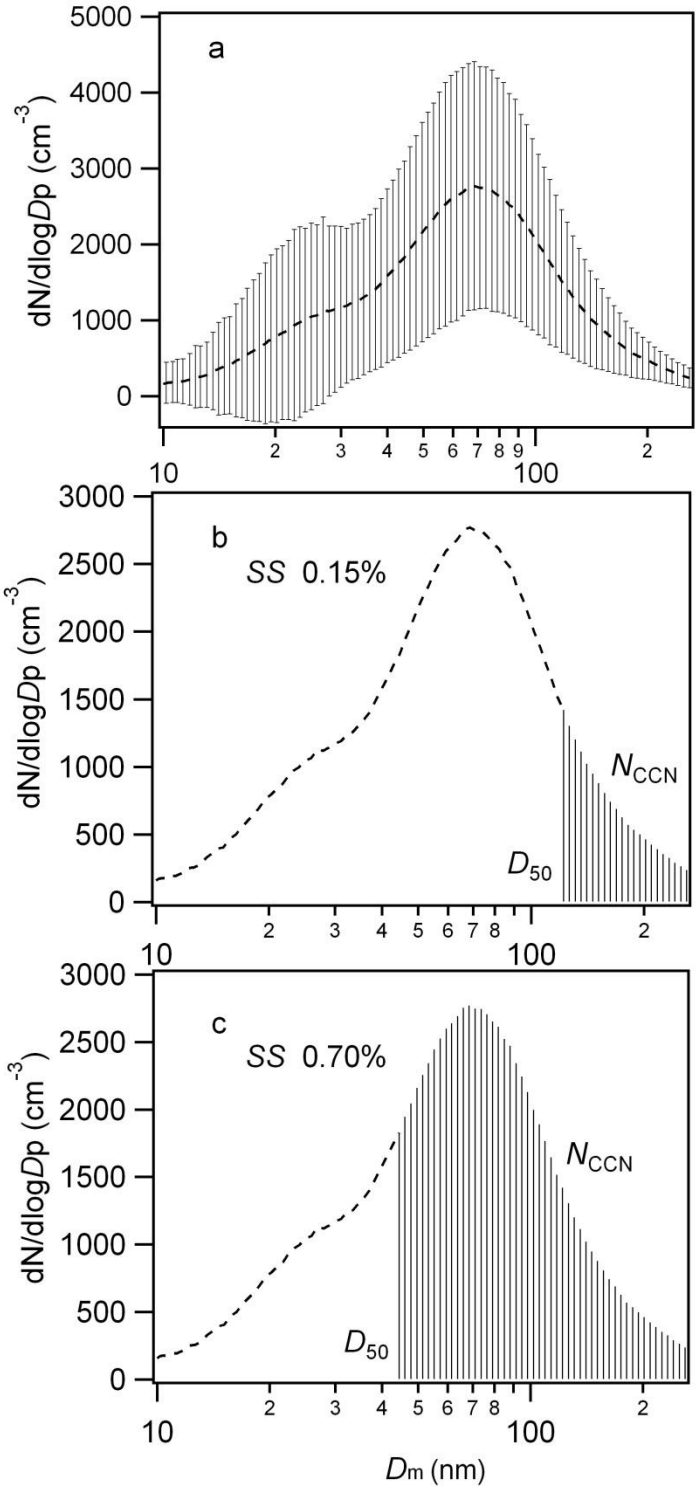

Fig.6. The average aerosol size distribution over the whole period (a), N_{CCN} prediction based on D_{50} at *SS* of (b) 0.15% and (c) 0.70%. Data points are mean values and standard deviation.

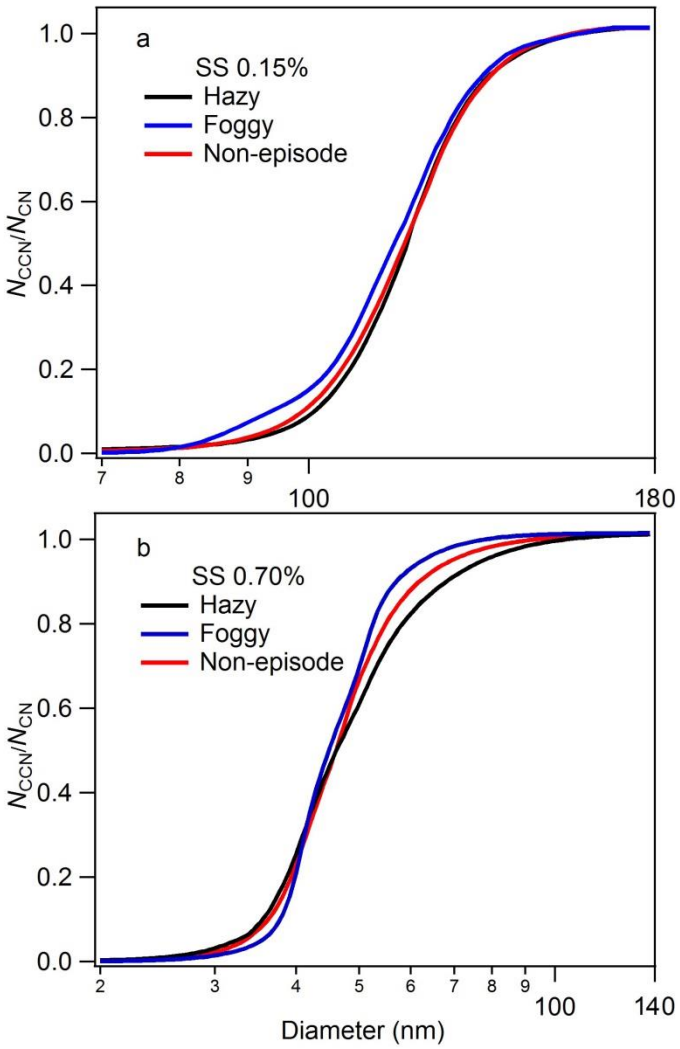

Fig.7. The average size-resolved CCN activation ratio at *SS* of (a) 0.15% and (b) 0.70% during the hazy, foggy and non-episode periods.

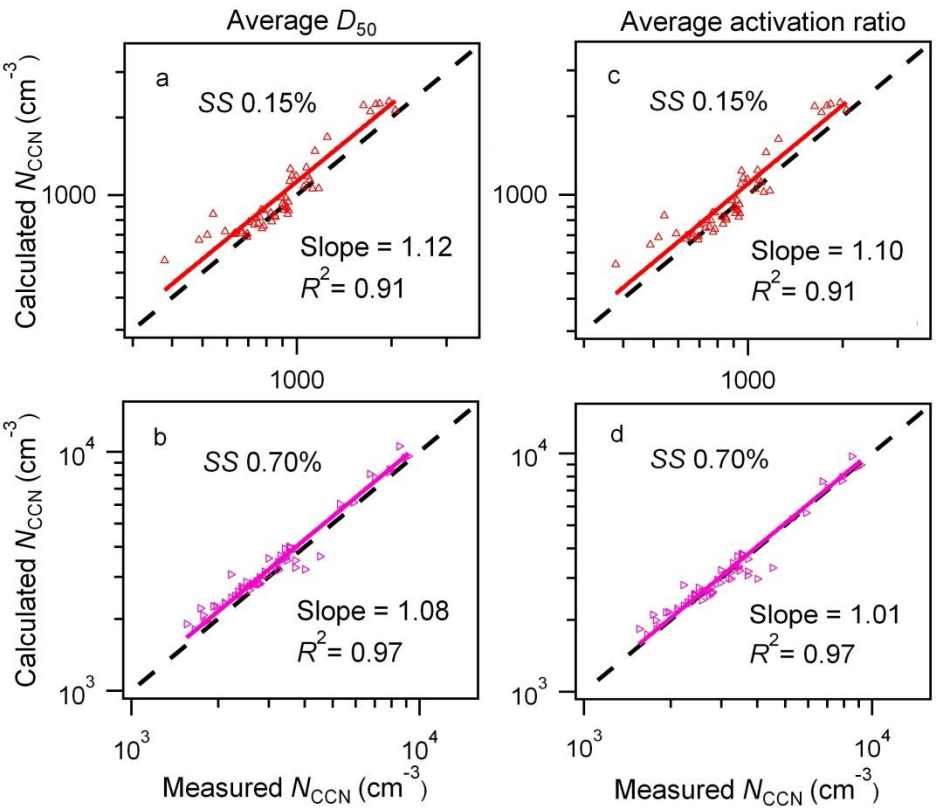

Fig.8. N_{CCN} estimations in the hazy period based on (a and b) the average D_{50} and (c and d) the average size-resolved CCN activation ratio from CCN measurement over the hazy period.